Superintermolecular orbitals in the C_{60}-pentacene complex

G. P. Zhang,[1,*] A. Gardner,[1] T. Latta,[1] K. Drake,[1] and Y. H. Bai[2]
[1]*Department of Physics, Indiana State University, Terre Haute, Indiana 47809, USA*
[2]*Office of Information Technology, Indiana State University, Terre Haute, Indiana 47809, USA*
(Received 28 September 2016; published 2 December 2016)

We report a group of unusually big molecular orbitals in the C_{60}-pentacene complex. Our first-principles density-functional calculation shows that these orbitals are very delocalized and cover both C_{60} and pentacene, which we call superintermolecular orbitals (SIMOs). Their spatial extension can reach 1 nm or larger. Optically, SIMOs are dark. Different from ordinary unoccupied molecular orbitals, SIMOs have a very weak Coulomb and exchange interaction. Their energy levels are very similar to the native superatomic molecular orbitals in $C_{60}$and can be approximately characterized by orbital angular momentum quantum numbers. They have a distinctive spatial preference. These features fit the key characters of charge-generation states that channel initially bound electrons and holes into free-charge carriers. Thus, our finding is important for C_{60}-pentacene photovoltaics.

DOI: 10.1103/PhysRevA.94.062501

I. INTRODUCTION

Organic solar cells are flexible, stretchable, and possibly wearable. If they could be integrated into our clothing, they would power our portable phones and computers. C_{60}-pentacene solar cells are a prime example in organic photovoltaics [1], where pentacene (Pc) serves as an electron donor and C_{60} serves as an electron acceptor. When light strikes pentacene, a complex singlet is formed and subsequently is split into two optically inactive triplets, or singlet fission [2–6]. Such a unique feature, where one single photon creates two triplets, greatly improves the quantum efficiency of charge photogeneration [7].

But the high quantum efficiency is only the first step for the photovoltaic cell [7]. What is more important is the states that channel initially bound electrons and holes into free charge carriers. Bakulin *et al.* [8] showed that the formation of delocalized states facilitates photoconversion. In 2014, Gelinas *et al.* [9] suggested that a rapid (40-fs) charge separation proceeds through delocalized π-electron states in ordered regions of the fullerene and acceptor material. Chen *et al.* [10] also found that charge photogeneration occurs predominantly via those delocalized hot exciton states. Paraecatti and Banerji [11] more directly pointed out that exciton delocalization provides an efficient charge separation pathway. These prior studies established beyond any doubt the importance of delocalized states, but what are these delocalized channel states [12,13]? To this question, there has been no obvious answer. That is the focus of our study.

In this paper, we carry out an extensive first-principles density-functional calculation to show that there is a group of unusually large superintermolecular orbitals (SIMOs) in the C_{60}-Pc complex that bridges both C_{60} and pentacene. We employ a real grid mesh method so we can treat both ordinary molecular orbitals and SIMOs on equal footing. We find that, energetically, SIMOs are close to native superatom molecular orbitals in C_{60}, but spatially, SIMOs are much larger, with spatial extension over 1 nm. They are optically silent. By computing over 3000 Coulomb and exchange integrals, we find that both Coulomb and exchange interactions among SIMOs are, in general, much smaller than those among ordinary molecular orbitals, a necessary condition to allow initially bound electrons and holes to dissociate into free charge carriers. Interestingly, regardless of edge-on and face-on geometries, SIMOs retain their original shapes. These features strongly suggest that they are good candidates for those channel states in C_{60}-Pc solar cells.

The rest of the paper is arranged as follows. In Sec. II, we present our theoretical formalism and the details of our first-principles calculation. Section III is devoted to the results and discussion. We conclude this paper in Sec. IV. The Appendix at end provides additional details about our hybrid message passing interface (MPI) and open multi-processing (OPEN-MP) parallel implementation.

II. METHOD

Our calculation is based on the first-principles density functional code OCTOPUS [14], which employs the pseudopotential method and the real grid mesh in real space and has the important advantage that it treats localized and delocalized states on an equal footing. To start with, we solve the Kohn-Sham (KS) equation in atomic units,

$$\left[-\tfrac{1}{2}\nabla^2 + V_{\text{eff}}(\mathbf{r})\right]\phi_i(\mathbf{r}) = E_i\phi_i(\mathbf{r}), \tag{1}$$

where $\phi_i(\mathbf{r})$ is the Kohn-Sham wave function and E_i is the eigenvalue of state i. The first term on the left-hand side of Eq. (1) is the kinetic-energy operator. The effective potential V_{eff} consists of the electron-nuclei interaction, the Hartree potential (due to the electron-electron Coulomb interaction), and exchange-correlation interactions,

$$V_{\text{eff}}(\mathbf{r}) = v(\mathbf{r}) + \int d\mathbf{r}'\frac{\rho(\mathbf{r}')}{|\mathbf{r}-\mathbf{r}'|} + V_{xc}(\mathbf{r}), \tag{2}$$

where the exchange-correlation potential V_{xc} is $\delta E_{xc}[\rho]/\delta\rho(\mathbf{r})$, taking the form of the local-density approximation (LDA). We find that LDA is sufficient for our purpose, and using the generalized gradient approximation (GGA) raises the energy by 0.5 eV [15]. The new charge density is computed by

*gpzhang@indstate.edu

summing over all the occupied orbitals N_{occ},

$$\rho(\mathbf{r}) = \sum_{i=1}^{N_{occ}} |\phi_i(\mathbf{r})|^2. \quad (3)$$

The next iteration starts. This process repeats itself until the charge density converges. With the converged wave function, we then compute the Coulomb and exchange integrals using National Energy Research Scientific Computing Center machines. However, these integrals over six degrees of freedom are extremely time-consuming, with so many mesh grid points (see the Appendix for details). We employ the submatrix technique, where we compute the action of the Coulomb term on states n and m and then multiply two additional wave functions in the above results. We develop a hybrid MPI-OPENMP code that breaks the integral into segments and distributes them to processors and nodes. Finally, the master node sums all the results up. This speeds up our calculation greatly.

We use the norm-conserving pseudopotential developed by Troullier and Martins [16]. Our simulation box is a cylinder. The radius of the cylinder is $r = 30$ Å, and the length is 80 Å. The grid mesh is $m = 0.22$ Å, and the total number of grid mesh points is 22 814 131. We have checked the convergence with the grid mesh and find that our results converge well. The C_{60}-pentacene complex has 342 valence electrons, so 171 orbitals are doubly occupied. To obtain those unoccupied states, we add 129 extra states (in OCTOPUS, the command is EXTRASTATES = 129), so we have eigenstates all the way up to 300. This covers the entire spectrum that is of interest to us. The threshold for the charge-density convergence is set to 10^{-4}, and the threshold for the absolute energy convergence is set to 5×10^{-7} eV. All the OCTOPUS calculations are run on our university Silicon cluster, where each computing node has dual Intel Xeon E5-2680 v2 CPUs with 2.80 GHz. Each CPU has 10 cores and cache size of 25 MB. The total memory for each node is 132 GB. The entire calculation needs 80 GB of memory and takes nearly two months to finish. After the calculation is finished, we export the wave functions from state number 97 up to 300 in two different formats, one for XCRYSDEN rendering of orbital images and the other in the Cartesian format. The latter is the actual wave functions in the three-dimensional space $\phi(x,y,z)$. These wave functions are extremely convenient for calculating other properties of interest.

III. RESULTS: SUPERINTERMOLECULAR ORBITALS

Photovoltaic effects depend on an efficient charge transfer from a donor D to an acceptor A [17]. Figure 1 schematically illustrates that light first strikes C_{60}-Pc but the subsequent charge transfer relies on channel states. While there is no detailed study of these channel states, several studies have estimated the size of channel states to be around 3–4 nm [9,18–22]. This distance corresponds to a binding energy of 0.1 eV, which can be reasonably approximated as $E_B = q^2/4\pi\epsilon r_{CT}$. Here q is the charge, and r_{CT} is the separation between average electrons and holes in the parent charge-transfer (CT) state. However, no ordinary molecular orbitals can be as big as 4 nm. Being unaware of the possible relevance to photovoltaics in C_{60}-Pc, Feng and her coworkers [23] reported some peculiar molecular orbitals in C_{60} resembling the atomic

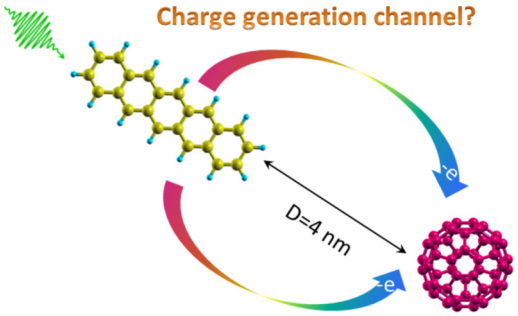

FIG. 1. Light first strikes the C_{60}-pentacene complex and creates a singlet, followed by singlet fission into triplets. But electrons and holes have to dissociate from each other to become free charge carriers. The central question is what the channel states are for charge generation in organic solar cells. We show that the superintermolecular orbitals may offer an answer.

orbitals but with a much larger radius. They are not localized around the atoms of the cluster, but rather, they belong to the entire cluster and thus are called superatomic molecular orbitals (SAMOs). Feng *et al.* detected these SAMOs using a scanning tunneling microscope (STM), where the voltage bias is gradually tuned. Their appearance is due to the partial delocality of outer shells of carbon atoms which jointly create a potential. Such a potential allows electrons to partially delocalize around the entire molecule. These orbitals have a distinctive shell structure from $1s$ up to $1d$ and are optically dark states. When we were investigating SAMOs [15], we were keenly aware of the large size of those SAMOs. We notice that the $1s$ orbital has a size close to C_{60} [15].

To begin with, we employ GAUSSIAN09 [24] to separately optimize C_{60}, pentacene, and C_{60}-Pc structures. We use the Becke, three-parameter, Lee-Yang-Parr (B3LYP) method and a correlation-consistent polarized valence double-zeta (cc-pVDZ) basis. The results are fully consistent with our and previous calculations [25,26] in both the eigenenergies and wave functions. The optimized coordinates in GAUSSIAN09, without further optimization, are used as an input for OCTOPUS [14]. The reason is that OCTOPUS uses a grid mesh and slightly breaks the symmetry of degenerate eigenstates. Although the change in energy is small, we worry that the introduced force may be too great if we use it to optimize our C_{60}-Pc complex.

As done by many researchers [27–30], we consider both edge-on and face-on configurations. In the edge-on configuration one end of Pc is aimed at the hexagons and/or pentagons on C_{60}, while in the face-on configuration, the plane of Pc faces the hexagons and/or pentagons on C_{60}.

A. Edge-on configuration

We start with the edge-on geometry. The distance between the frontier carbon atoms of Pc and the hexagons on C_{60} is 7.1 Å, larger than in previous investigations [27,31]. The distance between the far left carbon atoms on Pc and the far right carbon atoms on C_{60} is 19.3 Å. The left panel of Fig. 2 shows one example of the edge-on configuration. This is the wave function $\psi_{205}(\mathbf{r})$ for orbital 205 plotted at an isovalue of 0.005 $\sqrt[-3]{\text{Å}}$. The color difference denotes the sign of $\psi_{205}(\mathbf{r})$.

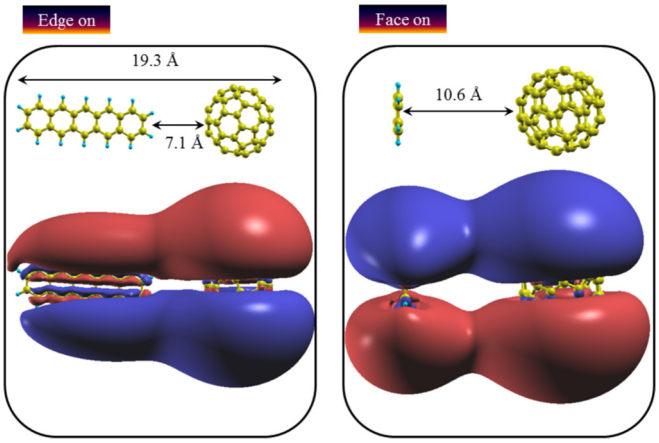

FIG. 2. Superintermolecular orbitals in C_{60}-pentacene for the edge-on configuration (left) and face-on configuration (right). We show one representative $1p$ SIMO for each configuration; $1p$ SIMO has orbital number 205.

Different from SAMOs [23], this superorbital covers both Pc and C_{60} molecules, hence the name superintermolecular orbital. In the language of SAMO, this could be $1p$ SIMO, but for SIMOs, the orbital character is approximate due to the symmetry reduction. We find that in general SIMOs have special orientations just as an ordinary molecular orbital. In some cases, SIMOs are more like SAMOs on an isolated C_{60}. This spatial preference is crucial since it allows the electrons to transfer from Pc to C_{60} unidirectionally. One special feature that is inherent in SAMOs is that the dipole transition matrix elements between SIMOs and ordinary molecular orbitals are very small. For this reason, we do not expect an optically induced charge transfer to occur from ordinary molecular orbitals to SIMOs. Instead, the initial bound exciton must dissociate into SIMOs through tunneling. We recall that Feng *et al.* [23] detected SAMOs using STM. The quantum tunneling is also closer to what happens in solar cells.

However, in photovoltaics, electrons are first excited into those low-lying lowest unoccupied molecular orbitals (LUMOs), which have been the focus of recent investigations. For free charge generation, the majority of theoretical studies start from an initial state $\phi_i^m(\mathbf{r})$ localized on D, where m is the multiplicity of state i and $\mathbf{r}$ is the electron coordinate. One hopes that this initial state ends up at a final state $\phi_f^n(\mathbf{r})$ localized on A. In the many-body picture [32], one often starts from configurations like

$$|\Psi\rangle = a\left|\phi_i^m(\mathbf{r}_1)\phi_f^n(\mathbf{r}_2)\right\rangle + \text{high-order terms}. \quad (4)$$

If $|\phi_i^m(\mathbf{r}_1)\phi_f^n(\mathbf{r}_2)\rangle$ takes a significant weight on the many-body wave function, CT is realized. This idea is simple and attractive but faces a dilemma. To have a large contribution from the configuration $|\phi_i^m(\mathbf{r}_1)\phi_f^n(\mathbf{r}_2)\rangle$, the Coulomb and exchange interaction matrix elements must be large, but this leads to a large binding energy, which is detrimental to free charge-carrier generation [33]. On the other hand, if the above elements are small, then the coupling is weak, and the transition to CT states is less likely. We compute all the Coulomb and exchange integrals from the LUMO up to LUMO+1; there are in total four orbitals since LUMOs are nearly degenerate. Table I shows all the Coulomb and exchange integrals among all the LUMO states. We find that the strongest interaction is 4.51 eV, which is more than 40 times larger than the disorder energy of 0.1 eV estimated by Clarke and Durrant [34]. This leads to a high binding energy for excitons; thus, it is detrimental to free charge-carrier generation [33]. This simple estimate highlights that states initially excited by the light are unlikely to be the same states that are responsible for final charge transfer and charge separation. A different group of states engages the final step of charge generations.

The above calculation is limited to only four unoccupied orbitals. Before we present results for C_{60}-Pc, we completely map out all the matrix elements for all the states from the highest occupied molecular orbital (HOMO)−4 through $1g$ SAMOs in native C_{60}. There are 3081 Coulomb and exchange integrals. All the calculations are carried out at Berkeley National Laboratory's National Energy Research Computing Center. Figure 3 shows a complete list of those matrix elements. Since these matrix elements are symmetric with respect to the state permutation (other combinations have a much smaller amplitude and thus are not shown), we show only the upper triangle for the Coulomb integral and the lower triangle for the exchange integral. Both the horizontal and vertical axes denote the states. The SAMO state labels are slightly off the axis for clarity. Along the horizontal axis, the second H_u state from the left is our HOMO, and the first T_{1u} is our LUMO. The radii of the circles are proportional to the magnitude of the integral. The Coulomb integrals are, in general, much larger, so when we plot them, we reduce their size by multiplying them by 0.15. A general pattern emerges. For ordinary molecular orbitals, the Coulomb and exchange integrals are much larger. The exchange integrals are much less uniform than the Coulomb integral since the former greatly depends on the phases of the wave functions. The SAMOs' integrals are also sizable, in particular for the $1s$ SAMO, but once we are above the $1p$ SAMO, both Coulomb and exchange integrals drop very quickly. This opens a door for delocalized and weakly interacting SAMOs to participate in the charge generating process.

TABLE I. Coulomb and exchange matrix elements (in eV) among LUMO (from 172 to 174) and LUMO+1 (175).

	$K(nm\|mn)$ (eV)				$J(nm\|nm)$ (eV)			
$n\backslash m$	172	173	174	175	172	173	174	175
172	3.64	3.42	3.42	0.92		0.107	0.107	0.555×10^{-6}
173	3.42	3.64	3.42	0.93	0.107		0.108	0.169×10^{-5}
174	3.42	3.42	3.64	0.92	0.107	0.018		0.916×10^{-6}
175	0.92	0.93	0.92	4.51	0.555×10^{-6}	0.169×10^{-5}	0.916×10^{-6}	

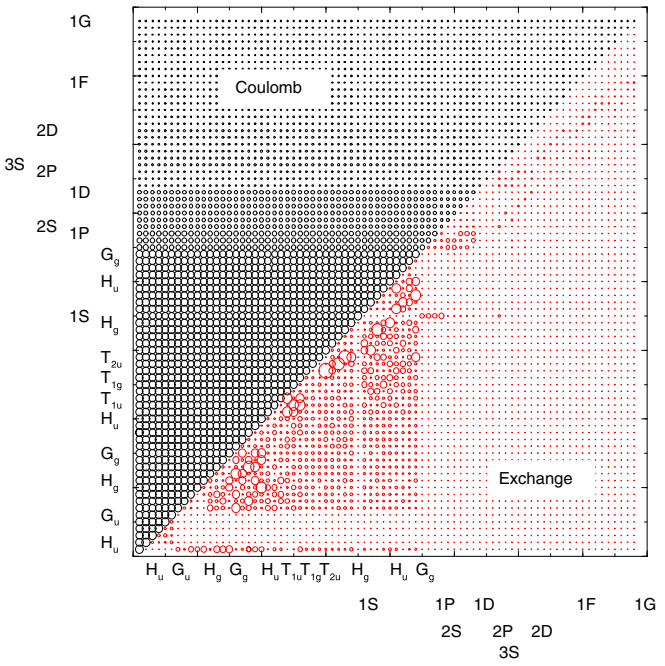

FIG. 3. Coulomb and exchange matrix elements between pairs of states in native C_{60}. There are 3081 elements. The magnitude of matrix elements is proportional to the radius of circles, and all the Coulomb elements are rescaled by multiplying by 0.15. Since the matrix is symmetric, the upper triangle shows the Coulomb integral, while the lower triangle shows the exchange integral.

To build a case for SIMOs, we also compute the Coulomb and exchange integrals, and we find that similar to SAMOs, their values are an order of magnitude smaller. Figure 4 compares the Coulomb (upper triangle) and exchange (lower triangle) integrals for LUMOs and SIMOs. The largest circle represents 4.51 eV (which is from LUMO+1). The Coulomb interaction drops quickly once we are above the 1*s* SIMO. The smallest Coulomb interaction is for $1f$ SIMOs, only 0.43 eV. If we consider the dielectric constant of the medium to be about 3, this interaction is reduced to 0.14 eV, very close to the disorder energy. These small Coulomb and exchange integrals are also reflected in the small transfer integral used by Smith and Chin [35]. They concluded that the transfer integrals are no larger than 8 meV, extremely tiny in comparison to those in C_{60} [36].

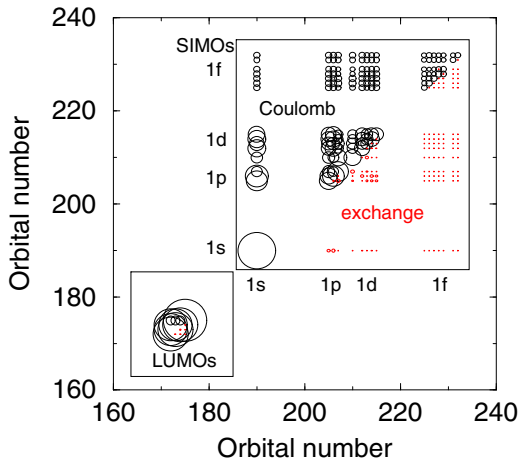

FIG. 4. Coulomb and exchange matrix elements between pairs of states. The magnitude of matrix elements is proportional to the radius of circles. Since the matrix is symmetric, the upper left triangle shows the Coulomb integral, while the lower right triangle shows the exchange integral. The largest Coulomb integral (4.51 eV) is from LUMO+1 (orbital number 175) localized on Pc, and the smallest (0.43 eV) is among $1f$ SIMOs (orbital numbers 226 and 228). The exchange integrals are shown by small red circles and are extremely small.

In 2016, in poly(3-hexylthiophene) and/or fullerene blends, D'Avino *et al.* [22] argued that the bound localized charge-transfer (LCT) states coexist with delocalized space-separated states because LCT states hybridize with singlets. In a later study [37], they also suggested that both C_{60} and its derivative may sustain high-energy states that spread over a few tens of molecules by pointing out sizable intermolecular delocalization of the electron wave function. Here our SIMOs present an alternative.

B. Face-on configuration

We also consider the face-on geometry. In this configuration, the distance between Pc and C_{60} is 10.6 Å, also larger than in many prior studies. This configuration is considered to be the most favorable one for the charge transfer and charge separation. The right panel of Fig. 2 shows the $1p$ SIMO. It is interesting that although the face-on geometry is so different from the edge-on geometry, the SIMO retains its shape well. The wave function in Pc has a larger amplitude than that for the edge-on configuration. This may explain why it is more efficient since the orbital is very delocalized. This meets one of the requirements for the channel states. Therefore, once an electron tunnels into this orbital, it has an excellent chance to transfer to C_{60}.

Energetically, the SIMOs appear in the same energy window as native SAMOs in C_{60}. Naturally, this also depends on the spatial orientation of Pc and C_{60}. Figure 5 (top panel) compares the SIMO energies in C_{60}-Pc with those of SAMOs in C_{60}. We see that the 1*s* SIMO and 1*s* SAMO are aligned with each other. However, the $1p$ SAMO is now split into three nearly degenerate levels due to the symmetry reductions, as explained above. The difference becomes bigger for $1d$ SIMOs. We see that the lowest $1d$ SIMO is shifted down by 0.16 eV. We understand why it is so. The bottom left panel shows that the orbital wave function is delocalized over Pc and C_{60} and there are nodal lines in between. The lobes of the orbital overlap strongly. This lowers the orbital energy significantly. By contrast, other orbitals do not change too much. The $1f$ SAMO is also split. To show the orbital 228 has f character, we rotate the complex structure so pentacene points out of the page. It is clear that the orbital retains the f character, but the orbital is elongated along the Pc-C_{60} axis. Quantitatively, the $1f$ SAMO in native C_{60} is at 0.204 eV, while the $1f$ SIMOs lie between 0.186 and 0.212 eV. Interestingly, Pavlyukha and Berakdar [38] showed that SAMOs are long-lived, coincident with the experimental observation [39]. This is what a channel state is supposed to be. These agreements constitute strong evidence that the

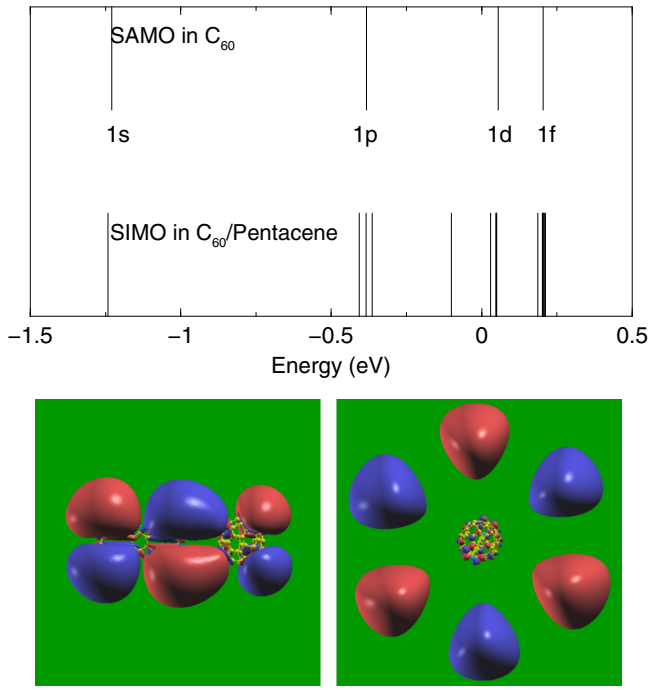

FIG. 5. Top: Energy-level comparison between SIMOs of C_{60}-pentacene and SAMOs of C_{60}. The energy in $1s$ states is similar. A small splitting is noticed in the $1p$ state. The $1d$ state has the largest shift of 0.16 eV due to an overlap in the d orbitals. Change in $1f$ is small. Bottom: Wave function of $1d$ SIMO (left) and wave function of $1f$ SIMO (right).

SIMOs may serve as a possible channel for charge separation. However, it is difficult to detect these delocalized excited states [40] optically since they may have a low absorption cross section [41]. One possible method to test our prediction is the transport measurement. Such a measurement is, in fact, more directly related to charge transfer in photovoltaics than the optical means. Finally, we notice that there is an ongoing debate on how or if hot charge-transfer excitons assist free carrier generation [42,43]. But even if hot CT excitons do play a role [33], the binding energy of an interfacial CT exciton after initial excitation is too high for the thermal activation to climb out of the Coulomb trap. We argue that SIMOs reported here may provide an alternative path to CT.

IV. CONCLUSIONS

We carried out the first-principles density-functional calculation in the C_{60}-Pc complex and found that there exists a group of big superintermolecular orbitals. These orbitals are very delocalized and cover both Pc and C_{60}. We found that SIMOs have the right spatial and energetic characters to channel the initially bound electrons and holes into free charge carriers. Spatially, they are much larger than ordinary molecular orbitals, close to 1 nm, a critical distance for CT. They have a clear spatial orientation from Pc to C_{60}, a crucial element that greatly facilitates triplet dissociation into free charge carriers. Energetically, both exchange and Coulomb interactions of SIMOs are very small, on the order of 0.1 eV, a value that matches the Clarke-Durrant disorder energy of 0.1 eV [34]. Thus, our finding highlights an unexpected benefit from SIMOs and points to a possible strategy for tailoring material properties toward high-efficiency organic solar cells. One possible method to enhance charge generation is to employ a larger fullerene, where SIMOs can be made even larger. This is consistent with the experiment [10], which showed that large fullerene crystals can enhance charge separation yields. We expect that our finding will motivate further experimental and theoretical investigations on these exciting opportunities at the frontier of photovoltaics.

ACKNOWLEDGMENTS

This work was supported by the U.S. Department of Energy under Contract No. DE-FG02-06ER46304 (G.P.Z.). This research used resources of the National Energy Research Scientific Computing Center, which is supported by the Office of Science of the U.S. Department of Energy under Contract No. DE-AC02-05CH11231.

APPENDIX: CALCULATION OF COULOMB AND EXCHANGE INTEGRALS

In this Appendix, we explain how the Coulomb and exchange integrations are done using a combination of MPI and OPENMP parallelization. The Coulomb integral is

$$K(nm|mn) = \frac{1}{4\pi\epsilon_0}\int_{-\infty}^{\infty}\int_{-\infty}^{\infty}\int_{-\infty}^{\infty} d\mathbf{r}_1 d\mathbf{r}_2 \psi_n^\dagger(\mathbf{r}_1)\psi_m^\dagger(\mathbf{r}_2) \times \frac{e^2}{r_{12}}\psi_m(\mathbf{r}_2)\psi_n(\mathbf{r}_1), \quad \text{(A1)}$$

and the exchange integral is

$$J(nm|nm) = \frac{1}{4\pi\epsilon_0}\int_{-\infty}^{\infty}\int_{-\infty}^{\infty}\int_{-\infty}^{\infty} d\mathbf{r}_1 d\mathbf{r}_2 \psi_n^\dagger(\mathbf{r}_1)\psi_m^\dagger(\mathbf{r}_2) \times \frac{e^2}{r_{12}}\psi_n(\mathbf{r}_2)\psi_m(\mathbf{r}_1), \quad \text{(A2)}$$

where ψ_n and ψ_m are the respective wave functions for states n and m, r_{12} is the distance between two electrons situated at positions $\mathbf{r}_1$ and $\mathbf{r}_2$, and e is the charge unit. Although we may use the medium permittivity in the above equations, we decide to use the permittivity in vacuum ϵ_0 so the reader can verify our results easily. Note that we consider only the paired states since other forms have a much smaller integral. The integral over $\mathbf{r}_2$ is parallelized using OPENMP and distributed evenly to processors in each MPI task. The integral over $\mathbf{r}_1$ is parallelized using MPI. The final results in each MPI task are summed up using a MPI reduction. The only serial part of the implementation is the file input and output (IO) and the input of the wave functions. Since the Coulomb and exchange integrals have singularity, the treatment requires some caution, although their overall contributions are small. Around the singularity, we replace the cube (grid mesh used in OCTOPUS) by a sphere. The spherical coordinate allows an analytic integration. Then we rescale the volume of the sphere to that of a cube. Finally, we add the integral back to the final sum. This method is very accurate.

The above implementation is postprocessed in our own code, not in OCTOPUS. The hybrid MPI-OPENMP calculation is set up according to the computing system hardware

structure. The supercomputer system Cori at the National Energy Research and Scientific Computing Center (NERSC) at Berkeley National Laboratory has dual CPUs with a total of 32 cores per node. With this system we run four MPI tasks and eight OPENMP threads on each node to obtain optimal performance.

[1] J.-L. Bredas, J. E. Norton, J. Cornil, and V. Coropceanu, Molecular understanding of organic solar cells: The challenges, Acc. Chem. Res. **42**, 1691 (2009).

[2] W.-L. Chan, M. Ligges, A. Jailaubekov, L. Kaake, L. Miaja-Avila, and X.-Y. Zhu, Observing the multiexciton state in singlet fission and ensuing ultrafast multielectron transfer, Science **334**, 1541 (2011).

[3] V. K. Thorsmolle, R. D. Averitt, J. Demsar, D. L. Smith, S. Tretiak, R. L. Martin, X. Chi, B. K. Crone, A. P. Ramirez, and A. J. Taylor, Morphology Effectively Controls Singlet-Triplet Exciton Relaxation and Charge Transport in Organic Semiconductors, Phys. Rev. Lett. **102**, 017401 (2009).

[4] P. M. Zimmerman, Z. Zhang, and C. B. Musgrave, Singlet fission in pentacene through multi-exciton quantum states, Nat. Chem. **2**, 648 (2010).

[5] M. W. B. Wilson, A. Rao, J. Clark, R. S. S. Kumar, D. Brida, G. Cerullo, and R. H. Friend, Ultrafast dynamics of exciton fission in polycrystalline pentacene, J. Am. Chem. Soc. **133**, 11830 (2011).

[6] S. N. Sanders, E. Kumarasamy, A. B. Pun, K. Appavoo, M. L. Steigerwald, L. M. Campos, and M. Y. Sfeir, Exciton correlations in intramolecular singlet fission, J. Am. Chem. Soc. **138**, 7289 (2016).

[7] D. N. Congreve, J. Lee, N. J. Thompson, E. Hontz, S. R. Yost, P. D. Reusswig, M. E. Bahlke, S. Reineke, T. Van Voorhis, and M. A. Baldo, External quantum efficiency above 100% in a singlet-exciton-fission-based organic photovoltaic cell, Science **340**, 334 (2013).

[8] A. A. Bakulin, A. Rao, V. G. Pavelyev, P. H. M. van Loosdrecht, M. S. Pshenichnikov, D. Niedzialek, J. Cornil, D. Beljonne, and R. H. Friend, The role of driving energy and delocalized stats for charge separation in organic semiconductors, Science **335**, 1340 (2012).

[9] S. Gelinas, A. Rao, A. Kumar, S. L. Smith, A. W. Chin, J. Clark, T. S. van der Poll, G. C. Bazan, and R. H. Friend, Ultrafast long-range charge separation in organic semiconductor photovoltaic diodes, Science **343**, 512 (2014).

[10] K. Chen, A. J. Barker, M. E. Reish, K. C. Cordon, and J. M. Hodgkiss, Broadband ultrafast photoluminescence spectroscopy resolves charge photogeneration via delocalized hot excitons in polymer:fullerene photovoltaic blends, J. Am. Chem. Soc. **135**, 18502 (2013).

[11] A. A. Paraecattil and N. Banerji, Charge separation pathways in a highly efficient polymer: Fullerene solar cell material, J. Am. Chem. Soc. **136**, 1472 (2014).

[12] B. M. Savoie, A. Rao, A. A. Bakulin, S. Gelinas, B. Movaghar, R. H. Friend, T. J. Marks, and M. A. Ratner, Unequal partnership: Asymmetric roles of polymeric donor and fullerene acceptor in generating free charge, J. Am. Chem. Soc. **136**, 2876 (2014).

[13] B. M. Savoie, N. E. Jackson, L. X. Chen, T. J. Marks, and M. A. Ratner, Mesocopic features of charge generation in organic semiconductors, Acc. Chem. Res. **47**, 3385 (2014).

[14] X. Andrade, J. Alberdi-Rodriguez, D. A. Strubbe, M. J. T. Oliveira, F. Nogueira, A. Castro, J. Muguerza, A. Arruabarrena, S. G. Louie, A. Aspuru-Guzik, A. Rubio, and M. A. L. Marques, TDDFT in massively parallel computer architectures: The OCTOPUS project, J. Phys. Condens. Matter **24**, 233202 (2012).

[15] G. P. Zhang, H. P. Zhu, Y. H. Bai, J. Bonacum, X. S. Wu, and T. F. George, Imaging superatomic molecular orbitals in a C_{60} molecule through four 800-nm photons, Int. J. Mod. Phys. B **29**, 1550115 (2015).

[16] N. Troullier and J. L. Martins, Efficient pseudopotentials for plane-wave calculations, Phys. Rev. B **43**, 1993 (1991).

[17] G. P. Zhang, R. T. Fu, X. Sun, K. H. Lee, and T. Y. Park, Photoinduced charge transfer in excited C_{60}, J. Phys. Chem. **99**, 12301 (1995).

[18] B. Bernardo, D. Cheyns, B. Verreet, R. D. Schaller, B. P. Rand, and N. C. Giebink, Delocalization and dielectric screening of charge transfer states in organic photovoltaic cells, Nat. Commun. **5**, 3245 (2014).

[19] A. J. Barker, K. Chen, and J. M. Hodgkiss, Distance distributions of photogenerated charge pairs in organic photovoltaic cells, J. Am. Chem. Soc. **136**, 12018 (2014).

[20] M. C. Heiber and A. Dhinojwala, Estimating the magnitude of exciton delocalization in regioregular P3HT, J. Phys. Chem. C **117**, 21627 (2013).

[21] G. J. Dutton and S. W. Robey, Distance dependence of exciton dissociation at a phthalocyanie-C_{60} interface, J. Phys. Chem. C **117**, 25414 (2013).

[22] G. D'Avino, L. Muccioli, Y. Olivier, and D. Beljonne, Charge separation and recombination at polymer-fullerene heterojunctions: Delocalization and hybridization effects, J. Phys. Chem. Lett. **7**, 536 (2016).

[23] M. Feng, J. Zhao, and H. Petek, Atomlike, hollow-core-bound molecular orbitals of C_{60}, Science **320**, 359 (2008).

[24] M. J. Frisch *et al.*, GAUSSIAN09, Gaussian Inc., Pittsburgh, PA, 2009.

[25] G. P. Zhang, D. A. Strubbe, S. G. Louie, and T. F. George, First-principles prediction of optical second-order harmonic generation in the endohedral $N@C_{60}$ compound, Phys. Rev. A **84**, 023837 (2011).

[26] J. O. Johansson, G. G. Henderson, F. Remacle, and E. E. B. Campbell, Angular-Resolved Photoelectron Spectroscopy of Superatom Orbitals of Fullerenes, Phys. Rev. Lett. **108**, 173401 (2012).

[27] Y. Yi, V. Coropceanu, and J.-L. Bredas, Exciton-dissociation and charge-recombination processes in pentacene/C_{60} solar cells: Theoretical insight into the impact of interface geometry, J. Am. Chem. Soc. **131**, 15777 (2009).

[28] B. Yang, Y. Yi, C.-R. Zhang, S. G. Aziz, V. Coropceanu, and J.-L. Bredas, Impact of electron delocalization on the nature of the charge-transfer states in model pentacene/C_{60} interfaces: A density functional theory study, J. Phys. Chem. C **118**, 27648 (2014).

[29] L.-H. Li, O. Y. Kontsevoi, and A. J. Freeman, Orientation-dependent electronic structures and optical properties of the P3HT:PCBM interface: A first-principles GW-BSE study, J. Phys. Chem. C **118**, 10263 (2014).

[30] S. M. Ryno, Y.-T. Fu, C. Risko, and J.-L. Bredas, Polarization energies at organic-organic interfaces: Impact on the charge separation barrier at donor-acceptor interfaces in organic solar cells, ACS Appl. Mater. Interfaces **8**, 15524 (2016).

[31] T. Minami, M. Nakano, and F. Castet, Nonempirically tuned long-range corrected density functional theory study on local and charge-transfer excitation energies in a pentacene/C_{60} model complex, J. Phys. Chem. Lett. **2**, 1725 (2011).

[32] A. V. Akimov and O. V. Prezhdo, Nonadiabatic dynamics of charge transfer and singlet fission at the pentacene/C_{60} interface, J. Am. Chem. Soc. **136**, 1599 (2014).

[33] A. E. Jailaubekov, A. P. Willard, J. R. Tritsch, W.-L. Chan, N. Sai, R. Gearba, L. G. Kaake, K. J. Williams, K. Leung, P. J. Rossky, and X. Y. Zhu, Hot charge-transfer excitons set the time limit for charge separation at donor/acceptor interfaces in organic photovoltaics, Nat. Mater. **12**, 66 (2013).

[34] T. M. Clarke and J. R. Durrant, Charge photogeneration in organic solar cells, Chem. Rev. **110**, 6736 (2010).

[35] S. L. Smith and A. W. Chin, Phonon-assisted ultrafast charge separation in the PCBM band structure, Phys. Rev. B **91**, 201302 (2015).

[36] G. P. Zhang, R. T. Fu, X. Sun, D. L. Lin, and T. F. George, Relaxation process of charge transfer in C_{60}, Phys. Rev. B **50**, 11976 (1994).

[37] G. D'Avino, Y. Olivier, L. Muccioli, and D. Beljonne, Do charges delocalize over multiple molecules in fullerene derivatives?, J. Mater. Chem. C **4**, 3747 (2016).

[38] Y. Pavlyukha and J. Berakdar, Communication: Superatom molecular orbitals: New types of long-lived electronic states, J. Chem. Phys. **135**, 201103 (2011).

[39] A. D. Chepelianskii, J. Wang, and R. H. Friend, Low-Temperature Transport Properties of Photogenerated Charges in Organic Materials, Phys. Rev. Lett. **112**, 126802 (2014).

[40] A. Rao, P. C. Y. Chow, S. Gelina, C. W. Schlenker, C.-Z. Li, H.-L. Yip, A. K.-Y. Jen, D. S. Ginger, and R. H. Friend, The role of spin in the kinetic control of recombination in organic photovoltaics, Nature (London) **500**, 435 (2013).

[41] F. E. Osterloh, M. A. Holmes, J. Zhao, L. Chang, S. Kawula, J. D. Roehling, and A. J. Moule, P3HT:PCBM bulk-heterojunctions: Observing interfacial and charge transfer states with surface photovoltage spectroscopy, J. Phys. Chem. C **118**, 14723 (2014).

[42] G. Nan, X. Zhang, and G. Lu, Do 'hot' charge-transfer excitons promote free carrier generation in organic photovoltaics? J. Phys. Chem. C **119**, 15028 (2015).

[43] X. Shen, G. Han, D. Fan, Y. Xie, and Y. Yi, Hot charge-transfer states determine exciton dissociation in the DTDCTB/C_{60} complex for organic solar cells: A theoretical insight, J. Phys. Chem. **119**, 11320 (2015).